PERGAMON

Continental Shelf Research 20 (2000) 2295–2323

CONTINENTAL SHELF RESEARCH

The shoreface-connected ridges along the central Dutch coast — part 1: field observations

Jan W.H. van de Meene[a,*], Leo C. van Rijn[a,b]

[a]*Institute for Marine and Atmospheric Research, Utrecht University, P.O. Box 80115, 3508 TC Utrecht, The Netherlands*

[b]*Delft Hydraulics, P.O. Box 177, 2600 MH Delft, The Netherlands*

Received 22 July 1994; received in revised form 1 April 1998; accepted 28 February 2000

Abstract

The hydrodynamic and sediment transport processes on the Dutch inner-shelf were studied on the basis of short- and medium-term (days, month) field experiments during fair-weather and storm conditions. The primary goal of this study was to identify the mechanisms that may be responsible for the formation and maintenance of the shoreface-connected ridges in the study area. The hydrodynamic field observations do not consistently support existing theoretical models explaining the formation of such ridges. Instead, the water motion appears to be dominated by wind- and density-driven effects. A review of literature indicates that other field studies also fail to observe the flow response expected from theory. Sediment transport during fair-weather is very episodic, with bed load transport slightly dominant over suspended load transport. The sediment transport processes during storms are dominated by the mean fluxes, with waves acting as a stirring mechanism. The contribution of wave-oscillatory fluxes cannot be neglected and may be directed with and against the waves. Long-wave fluxes are present, but very small. © 2000 Elsevier Science Ltd. All rights reserved.

1. Introduction

The inner-shelf along the central Dutch coast is covered with a system of large linear sand banks, connected to the shoreface and oriented obliquely with respect to the dominant, coast-parallel tidal current (Fig. 1). Such sand bodies are prominent features on both tide- and storm-dominated continental shelves. If sufficient sand is

*Corresponding author. Present address: Royal Boskalis Westminster NV, P.O. Box 43, 3350 AA Papendrecht, The Netherlands. Tel.: +31-78-6969000; fax: +31-78-6969555.

0278-4343/00/$ - see front matter © 2000 Elsevier Science Ltd. All rights reserved.
PII: S0278-4343(00)00048-0

available and if the hydrodynamic processes are intensive enough to move the sediment, the sand banks form a morphodynamic system (e.g. Huthnance, 1982; Boczar-Karakiewicz and Bona, 1986; De Vriend, 1990; Boczar-Karakiewicz et al., 1990, 1991; Hulscher et al., 1993). Although many studies have focused on the morphodynamic behaviour of such sand bodies (for reviews see e.g. Pattiaratchi and Collins, 1987; Wright, 1995; Dyer and Huntley, 1999), there is no general consensus on the processes that may be responsible for their formation and their present day maintenance.

The difficulty in understanding the formation and maintenance of linear sand banks or ridges is caused, amongst others, by their scale. With typical length scales in the order of tens of kilometres and typical time scales in the order of centuries or millennia, the sand bodies are hard to study experimentally. Also, the environment in which they occur, the inner-shelf, is a complex area with respect to the sediment transport processes and the various forces that drive these processes. There may be a variety of processes active on the inner-shelf, but they are not necessarily all relevant to the formation and maintenance of the sand bodies. Distinguishing between regional effects, independent of and indifferent to sand bank maintenance, and local, sand bank related processes, may be difficult if not impossible. Also, sand banks or ridges may have multiple origins. Some may be relict, while some may have formed in the present environment. Relict ridges, in addition, may still be subject to present day reworking and maintenance.

The objective of the present study was to obtain a better understanding of the complex hydrodynamic and sediment transport processes on the Dutch inner-shelf and the resulting morphological behaviour of the shoreface-connected ridges in this area. This was done on the basis of short- and medium-term (days, months) hydrodynamic and sediment transport observations, collected during an extensive field study (Part 1 of this paper). In addition, model calculations were done to explore the long-term (decades, centuries) behaviour of the ridges (Part 2, Van de Meene and Van Rijn, 2000).

The study of linear sand banks such as the shoreface-connected ridges is of practical relevance as well. The behaviour of sand ridges, and especially their growth and mobility, are important for the planning and design of shipping lanes, shipping channels, pipelines and marine infrastructure such as artificial islands. Also, the large amounts of sand stored in these ridges may form a useful resource for sand mining for beach nourishment and land reclamation.

2. Sand bank dynamics and sediment transport processes

2.1. General

Linear sand bodies are found in a variety of geomorphological settings (e.g. Off, 1963; Belderson, 1986; Pattiaratchi and Collins, 1987; Wright, 1995; Dyer and Huntley, 1999). They occur in open shelf seas, adjacent to convergent or divergent coastlines (straits), in estuaries, often radiating from the distributary mouths, and off

coastal headlands. Linear sand bodies in open shelf seas are often divided into linear (tidal) sand banks, found in tide-dominated settings, and sand ridges, observed in storm-dominated settings. Shoreface-connected ridges have been considered a special class of storm-generated ridges, but the shoreface-connected ridges along the Dutch coast are found in a setting where tidal currents and storms may both be important. This suggests that a storm-dominated setting is not essential for the formation of shoreface-connected ridges. Reviews of shoreface-connected ridges have been given by e.g. Swift et al. (1978), Swift and Field (1981), McBride and Moslow (1991), Van de Meene (1994) and Van Rijn (1998).

It has been argued that there are significant morphological differences between active tide-dominated sand banks and storm-dominated sand ridges. The orientation of the tidal sand banks is related primarily to the peak tidal current direction, while the orientation of the storm sand ridges is related primarily to the orientation of the coastline. Tidal sand banks are generally higher than storm sand ridges: the former have heights up to 43 m, while the latter range between 3 and 12 m. Tidal sand banks may be steeper (6° or less) than storm sand ridges (2° or less) and they generally have sharper crests. Tidal sand banks have larger spacings than storm ridges and they are generally longer. Typical spacings range between 2 and 30 km for tidal sand banks and between 0.5 and 7 km for storm sand ridges. Tidal sand banks are up to 70 km long, storm sand ridges up to 20 km. These morphological differences suggest a genetic difference between the two ridge types. However, for both ridge types the mode of formation and maintenance is still not clear, and in both settings currents (tide- or wind-driven) as well as wind waves may affect sediment mobility.

An important feature of many sand bank systems is the lateral coherence of the individual sand bodies. Shelf sand bodies almost always occur in fields, often with a very constant spacing between the ridges. Although the factors controlling this lateral coherence are still largely unknown, three possible modes of formation of ridge fields have been recognized. Sand bank systems may have formed diachronously, as a response to a steady change in conditions such as flooding of an area and shoreface retreat due to sea-level rise. Alternatively, they may have formed simultaneously, as a response of the sea bed to a suitable hydraulic regime, or by the process of 'sand bank multiplication'.

There are a variety of theories and models that may explain the formation and maintenance of large sand banks or ridges. Firstly, there are geomorphological and geological theories, based on geomorphological and geological field observations (e.g. Swift and Field, 1981; Stubblefield et al., 1984; McBride and Moslow, 1991; Rine et al., 1991). These theories form descriptive and inductive models, usually lacking any theoretical or observational hydrodynamical basis. Secondly, there are mathematical models, describing the evolution of the sea bed as a result of interactions between water motion, sediment transport and bed-level changes, using well-established sets of mathematical formulations (e.g. Huthnance, 1982; De Vriend, 1990; Boczar-Karakiewicz and Bona, 1986; Boczar-Karakiewicz et al., 1990, 1991; Hulscher et al., 1993).

Two major types of mathematical models may be identified: bed-instability models and morphodynamic models. The bed-instability models explain the formation of

sand banks from the linear and non-linear interaction between the tidal current (with or without short waves) and the sea bed. Morphodynamic models explain the formation and maintenance of sand banks by computing the hydrodynamics, sediment transport rates and bed evolution in a continuous loop.

2.2. Geomorphological and geological theories of ridge formation

Geomorphological and geological theories of ridge formation have mainly focused on three effects: sea-level rise; relict origin and shelf environment.

Hypotheses of sea-level rise and associated shoreline retreat being the driving force in ridge formation originate predominantly from extensive studies along the east coast of the USA (e.g. Swift et al., 1978; Swift and Field, 1981; McBride and Moslow, 1991). The linear ridges on the American Atlantic shelves are often referred to as storm-generated ridges, consisting of three different types: shoreface-connected ridges, nearshore ridges and offshore ridges. The ridges generally rest on a marine transgression surface. Most authors agree that they originate at the shoreface and — as the shoreface retreats landwards due to sea-level rise — eventually become detached and isolated, thus evolving into nearshore and offshore ridges. The similarity of the ridges may suggest a single mode of formation for all ridges.

Several authors have argued that the ridges may have a relict origin, with present day reworking still being important. Others have concluded that the mid-shelf ridges are degraded barriers that are being modified by shelf currents, whereas the nearshore ridges are post-transgressive features formed as shoreface ridges. McBride and Moslow (1991) have compared the occurrence of shoreface-connected ridges with that of historical and active tidal inlets. They hypothesize that abandoned ebb-tidal deltas are the concentrated sinks of sand from which many shoreface ridges develop.

Houbolt (1968) and Laban and Schüttenhelm (1981) have demonstrated that some of the ridges found on the North Sea (part of the Zeeland Banks; banks in the Thames estuary) have a relict core, consisting of pre-transgressive material.

2.3. Mathematical bed-instability models

Theoretical analyses of the morphological behaviour of the sea bed have been presented by Huthnance (1982), De Vriend (1990), Hulscher et al. (1993), and Hulscher (1996). These authors have shown that the sea bed has an inherent tendency to become unstable, due to the interaction between water motion, sediment transport and morphological evolution.

The models are used to analyse the conditions (parameter settings) under which sand banks are predicted to grow and the dimension of the sand banks that are expected to survive. The models in this way serve as conceptual models, allowing for a qualitative analysis of the interactions in the morpodynamic system and an evaluation of hypotheses that may explain sand bank formation.

The model of Huthnance predicts sand bank growth for a wide range of wave numbers k and orientations α, with a broad maximum near $\alpha \approx \pm 28^\circ$ and $k = 10$ (corresponding to a morphological wavelength of about 250 times the water depth).

Ridge growth is caused by the oblique orientation of the sand bank with respect to the tidal current.

The model of De Vriend indicates that growth of sand banks orientated obliquely to the flow is predicted for any combination of tidal velocity amplitude, mean water depth, bottom roughness and sediment transport. This means that — for the model to be correct — the *presence* of such ridges in a tidal setting like the North Sea, rather than *absence* would be the normal situation.

2.4. Mathematical morphodynamic models

Morphodynamic models usually start from a number of standard models of constituent physical processes (waves, currents, sand transport), which are coupled via a bottom evolution module based on sediment conservation. An overview of two-dimensional horizontal (depth-averaged) and quasi-three-dimensional models has been given by De Vriend et al. (1993).

A one-dimensional approach including non-linear wave theory has been given by Boczar-Karakiewicz and co-workers. Using this approach, bar formation is explained from the interaction between bed modulations and the non-linear response of different types of waves (Boczar-Karakiewicz and Bona, 1986; Boczar-Karakiewicz et al., 1990, 1991). The waves modulate the sediment fluxes stirred by themselves or by any other mechanism (e.g. wind waves). The modulating waves may be either swell waves, infragravity or internal tidal waves. This type of models requires that the characteristics of the modulating waves are relatively constant in time, while they neglect the effects of wave reflection and refraction and of tidal currents.

2.5. Sediment transport processes on the inner shelf

Sand can be transported by wind-, wave-, tide- and density-driven currents (current-related transport), or by the oscillatory water motion itself (wave-related transport). Wave-related transport, for example, may be caused by the deformation of short waves under the influence of decreasing water depth (wave asymmetry) or by a combination of currents and short waves. The latter generally acts as a sediment stirring agent, whereas the sediments are transported by the mean current. Low-frequency waves interacting with short waves may also contribute to the sediment transport process. In friction-dominated deeper water on the inner shelf-zone the transport process is generally concentrated in a layer close to the sea bed and mainly takes place as bed-load transport in close interaction with small bed forms (ripples). Bed load transport is dominant in areas where the mean currents are relatively weak compared to the wave motion (small ratio of depth-averaged velocity and peak orbital velocity). Net sediment transport by the oscillatory motion is relatively small in depths larger than 10–15 m (Van Rijn, 1997), because the wave motion is rather symmetrical. Suspension of sediments can be generated by ripple-related vortices. Suspended load transport will become increasingly important with increasing strength of the tide- and wind-driven mean current, due to the turbulence-related mixing capacity of the mean current (shearing in

boundary layer). By this mechanism the sediments will be mixed up from the bed load layer to the upper layers of the flow.

3. Morphology and hydrography of the study area

The shoreface-connected ridges along the central Dutch coast (Fig. 1) are up to 30 km long, up to 2–4 km wide and between 2 and 6 m high. They are situated in water depths between 14 and 18 m. Typical wave length – water depth ratios are in the order of 230, which is close to the value found by Huthnance (1982). The mean grainsize of the sediments in the area ranges between 250 and 300 μm.

Measurements indicate that tidal currents and wind waves are both important sediment stirring agents (Van de Meene, 1994). The tidal amplitude varies between 1.5 m (neap tide) and 2 m (spring tide). The maximum surface tidal currents vary between 0.7 and 1.1 m/s, while the near-bed current velocities (1 m above the bed) are between 0.2 and 0.5 m/s. The northward directed flood current is dominant.

The residual (tide-averaged) water motion is dominated by wind- and density-driven effects (Van de Meene, 1994). The wind generates along-shore currents in the direction of the along-shore wind component, while it creates a vertical circulation in cross-shore direction driven by the cross-shore wind component (wind set-up and wind set-down). Due to fresh water inflow of the river Rhine, south of the study area, there is a persistent cross-shore horizontal density gradient in the study area. This density gradient gives rise to an estuarine type of vertical circulation, with near-bed residual currents directed towards the coast, compensated by a return flow higher in the vertical. Both wind- and density-driven residual currents reach values up to 0.10 m/s, while long-term (30 d) averages are between 0.03 and 0.05 m/s.

The mean annual wave height measured at a nearby station (Meetpost Noordwijk, Fig. 1) is 1.1 m, while wave heights larger than 3.5 m occur for 2% of the time. Wave orbital velocities at about 0.5 m above the bed ranging between 1 and 1.5 m/s were measured during regular winter storms, when waves are typically 3–4 m high (Van de Meene, 1994).

4. Hydrodynamic observations (currents and waves)

4.1. Introduction

The validity of the mathematical models introduced in Section 2 can be investigated by comparing the flow response predicted by these models with what is observed in nature. The basic flow response underlying the bed-instability models of e.g. Huthnance (1982) and De Vriend (1990) is represented schematically and qualitatively in Fig. 2, while a more elaborate and quantitative analysis is presented in Part 2 of this paper (Van de Meene and Van Rijn, 2000). The most conspicuous effects of tidal currents crossing a sand bank obliquely are (Fig. 2):

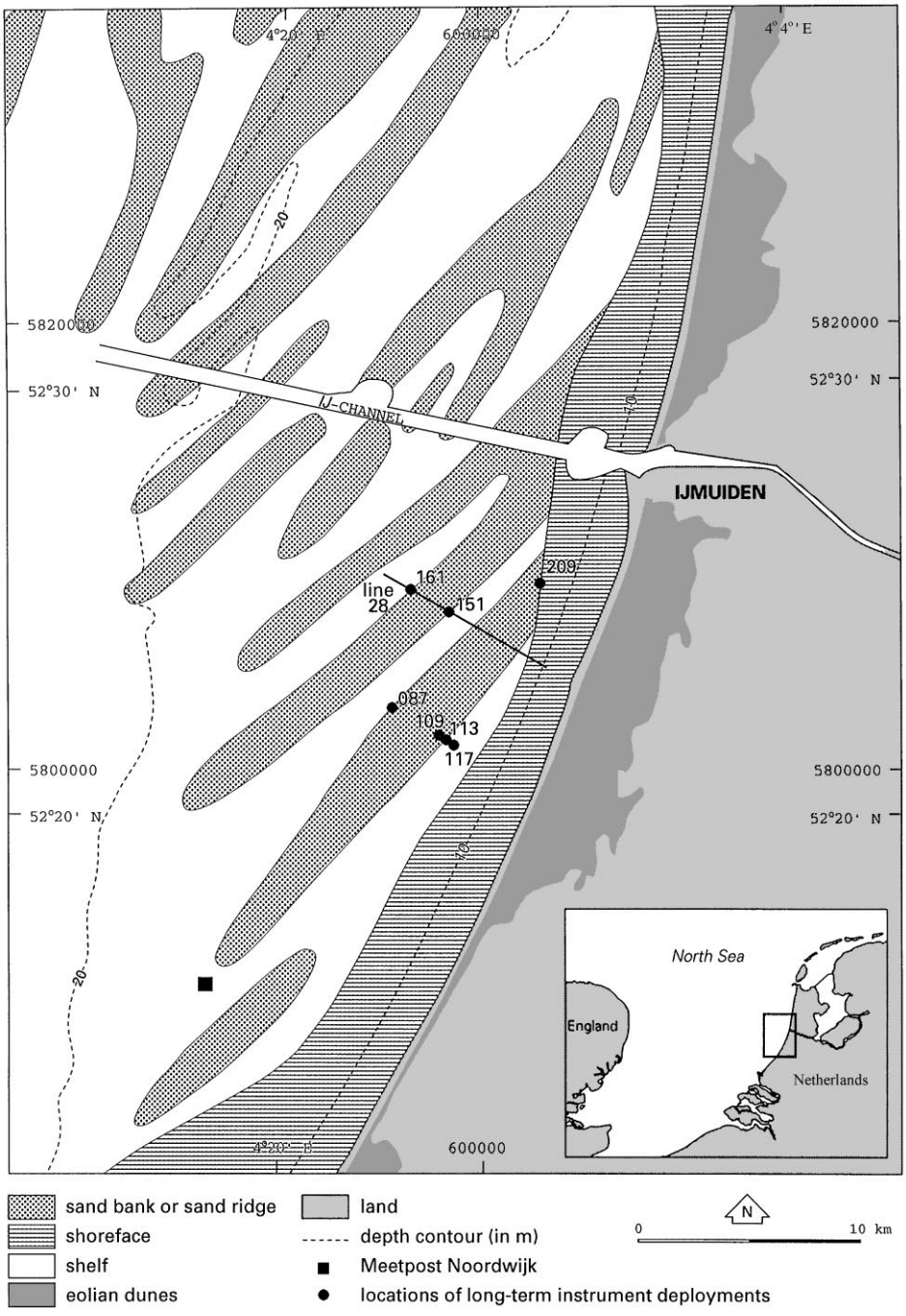

Fig. 1. Shoreface-connected ridges along the central Dutch coast, measurement locations.

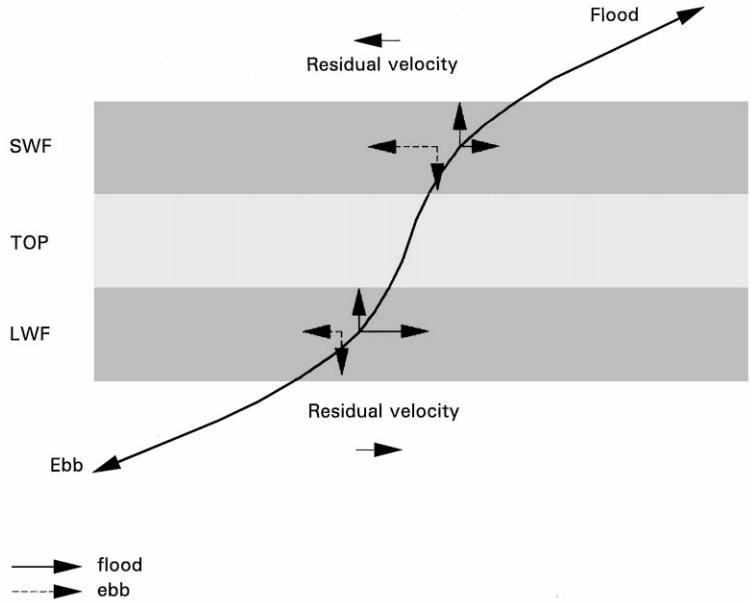

Fig. 2. Theoretical flow response across a tidal sand bank: LWF = landward flank (upcurrent during flood, downcurrent during ebb); TOP = top of the ridge; SWF = seaward flank (downcurrent during flood, upcurrent during ebb).

- current veering towards the crest, due to an increase of bottom friction with decreasing water depth;
- a decrease of the along-bank and total current velocity due to an increase of bottom friction;
- an increase in cross-bank velocity to satisfy continuity;
- a residual (tide-averaged) circulation around the ridges resulting from the above velocity variations.

The current observations in this section are used to evaluate to what extent the theoretical flow response can be observed in nature. Wave observations are used to obtain an idea to what extent the morphodynamic models of Boczar-Karakiewicz and co-workers may apply for the Dutch situation.

4.2. Current observations

4.2.1. Experimental set-up

The three-dimensional current structure is described on the basis of field observations from an acoustic doppler current profiler (ADCP) and several short- and long-term current meter deployments. In addition, vertical salinity distributions along the ADCP-transects were measured with a CTD probe (conductivity, temperature

and depth). Supporting data include wind velocities recorded routinely near Meetpost Noordwijk (Fig. 1) and discharge data of the river Rhine (Van de Meene, 1994).

The ADCP data were collected between 30 May and 1 June 1990, during fair-weather, spring tidal conditions. The measurements were done with a ship-borne 1200 kHz. ADCP along (amongst others) transect 28 (Fig. 1) for one tidal period (13 h). Traverses along this line were repeated once every hour.

Long-term current and water-level measurements were done near the locations depicted in Fig. 1. The measurements were carried out with NBA-2DNC current meters and Dag6000 pressure sensors. The instruments were deployed during six different periods between 1989 and 1991. The duration of the deployments was usually one month, but it varied between two weeks and two months. One experiment was done during fair-weather conditions (May–June 1990), the other five during generally stormy winter conditions (November–February).

All velocity observations were transformed into velocity components perpendicular and parallel to the main orientation of the sand banks. This crest orientation was taken 40–220° with the positive x-axis directed shoreward. The orientation of the coast line in this area is about 22–202°N.

4.2.2. Synoptic tidal current patterns (ADCP)

The cross-bank velocity pattern shows a clear velocity increase above the bank crests ('ac') during ebb (Fig. 3(a)) and a much more irregular pattern during flood (Fig. 3(b)). The along-bank velocity pattern (Figs. 3(c) and (d)) shows a velocity decrease downstream of the bank crest ('dc') during both ebb and flood. The depth-averaged velocity variations (decrease or increase) are between 0.05 and 0.15 m/s, which are significant variations given the random error in the velocity data of 0.02–0.03 m/s (Van de Meene, 1994). During flood, the along-bank velocity isolines are more or less parallel to the topography, contrasting with the much more irregular ebb-pattern.

The observed cross-bank and along-bank velocity variations agree partially and only qualitatively with the theoretical flow response of Fig. 2. A satisfactory explanation for the discrepancies cannot be given. Possible factors that may play a role are the finite length of the ridges, the presence of the coastline, the fact that the ridges are connected to the shoreface and the gentle but regional slope of the sea bed, from the shoreface to deeper water further offshore. These morphological phenomena are not taken into account in the models.

In addition, relatively strong horizontal density gradients and weak stratification observed during the measurements also affected the water motion. The horizontal density gradients induce a shoreward directed residual current close to the bed, compensated by a return flow higher in the profile (Van der Giessen et al., 1990; Van de Meene, 1994).

4.2.3. The tidal current pattern

A scatter plot of the current velocity at 1 m above the bed near MP 151 (Fig. 4) shows an oblique orientation of the current with respect to both sand bank and coast line. This indicates that the tidal current is being deflected by the ridge topography, as predicted by theory (Fig. 2). The absolute value of the inclination of the tidal

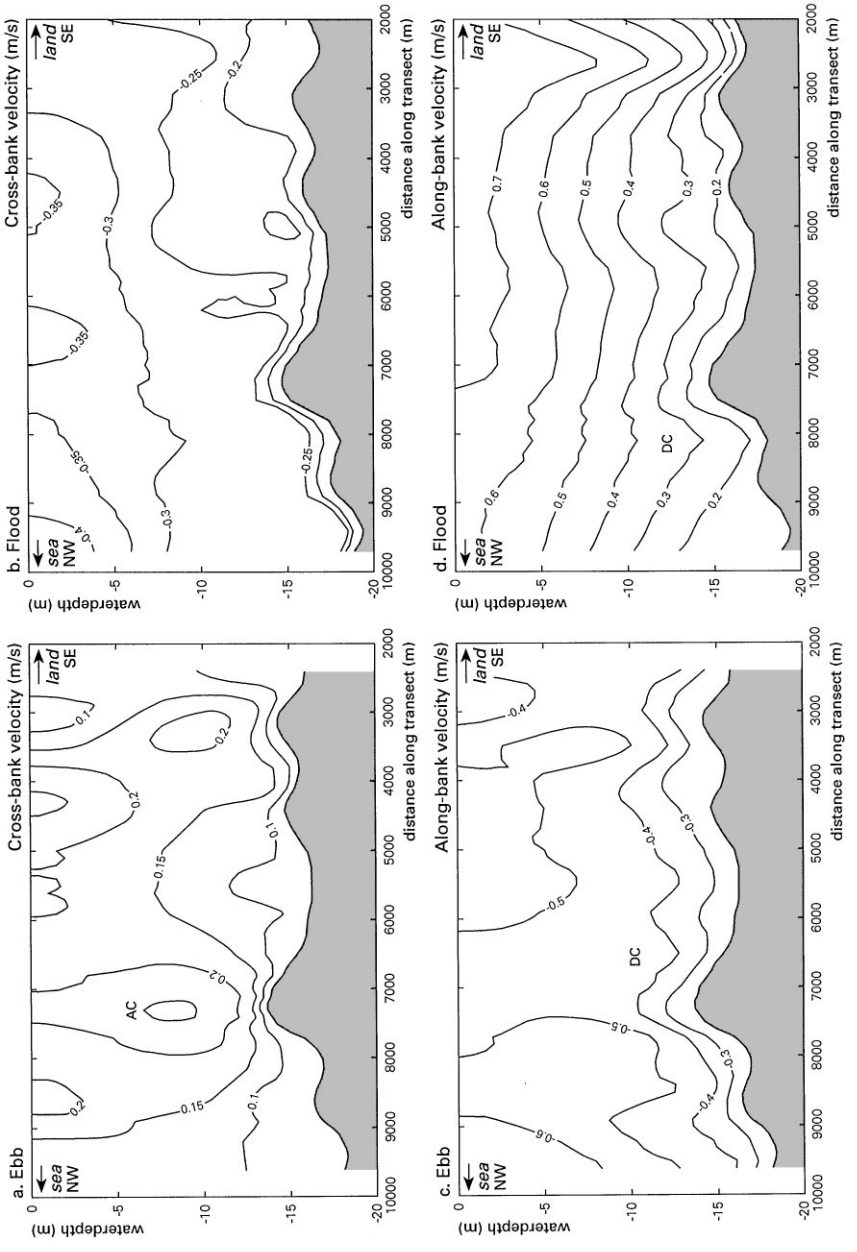

Fig. 3. ADCP observations along line 28 on 31 May 1990: (a) ebb, cross-bank; (b) flood, cross-bank; (c) ebb, along-bank; and (d) flood, along-bank.

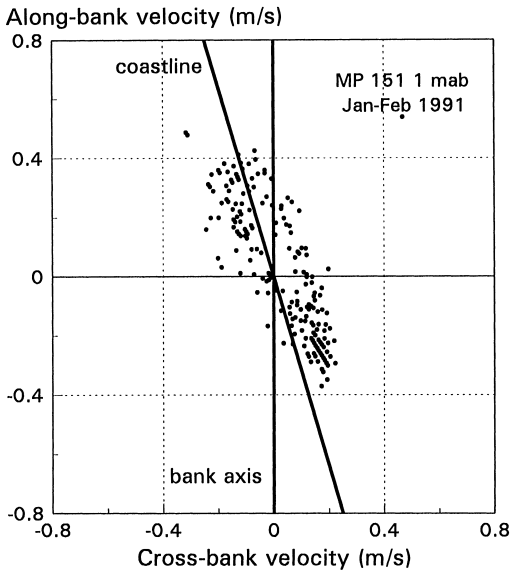

Fig. 4. Scatter plot of the tidal currents at 1 m above the bed near MP 151. Orientation coastline indicated in figure, bank-axis corresponds with Y-axis.

Table 1
Significant tidal current direction and current veering near MP 151

	θ_{bed} (°N)	$\theta_{mid-depth}$ (°N)	$\theta_{mid-depth}-\theta_{bed}$[a] (°)	n (−)
Jan–Feb				
Flood	22 ± 7	16 ± 7	-6 ± 4	141
Ebb	194 ± 3	193 ± 3	-1 ± 3	144
Nov–Dec				
Flood	34 ± 8	11 ± 4	-23 ± 6	63
Ebb	196 ± 4	190 ± 6	-6 ± 5	76

[a] Negative values indicate that the current veers towards the right (clockwise) in downward direction. Measurements were done in 1991. Indices refer to measurement height above the bed: 1 m (bed), 7 m (mid-depth, Jan–Feb); 9 m (mid-depth, Nov–Dec). θ is the current direction with respect to geographical North.

current with respect to the bank axis (around 30°) corresponds well with the inclination predicted by the stability analysis of Huthnance (1982). The sense of orientation however does not, as the shoreface-connected ridges are offset clockwise with respect to the tidal current.

During all measurements with simultaneous observations near the bed and at mid-depth, the current veering (vertical variation in current direction) was towards the right (clockwise in downward direction), both during ebb and flood (Table 1). Generally, the veering was in the order of a few degrees, differing from zero in all cases

(t-test, 0.99 significance level). The flood phase during the November–December period reveals a suspiciously large veering. However, there were no indications of instrument malfunctioning. The observed consistent clockwise veering towards the sea bed suggests that there are no vertical circulations near the sand banks. If such vertical circulations were present, the current veering in downward direction ($\theta_{surface} - \theta_{bottom}$) would be expected to change sign consistently for different tidal phases (ebb–flood) on one side of the bank and for the same tidal phase on either side of the bank (Heathershaw and Hammond, 1980; Pattiaratchi and Collins, 1987). The clockwise veering in the Zandvoort area contrasts with the current veering observed by McCave (1979) in the Southern North Sea and Heathershaw and Hammond (1980) in the Bristol Channel. These authors found a consistent anti-clockwise veering towards the sea bed, which they attributed to Ekman veering.

4.2.4. The residual current pattern

The long-term mean residual current pattern in the study area is given in Fig. 5. This figure gives the near-bed and mid-depth Eulerian residual current pattern, using the entire dataset of current meter deployments (1989–1991). Each residual current vector represents the average current velocity calculated over the entire length of the individual time-series. These time-series usually covered one month, but their length varied between two weeks and two months.

The long-term residual current pattern forms the net result of tidal flows, morphological effects and wind- and density-driven currents. Relevant for this study is whether the actual pattern reveals any indication of residual eddies circulating around the sand banks, as expected from theory (Fig. 2). The current pattern of Fig. 5 clearly does not give such an evidence for morphological steering. Instead, two other trends can be distinguished. Firstly, almost all residual vectors have a northward component, reflecting the regional flood dominance in the area. Secondly, there is a clear vertical variation in the residual current direction, with most near-bed vectors having a distinct shoreward component and most mid-depth vectors showing a seaward component, albeit with considerable scatter. This vertical variation in cross-shore direction is attributed to an estuarine-type density-driven circulation. Most near-bed shoreward directed residual velocity vectors are generally very steady, indicating that this density-driven effect is very persistent.

The effect of wind on the residual current pattern was studied qualitatively by removing the tidal components from the time-series with a low-pass filter (Godin, 1972). These low-pass-filtered current velocities roughly correlate with the wind velocity in two different ways. Strong northward directed winds enhance the northward directed tidal residual current, while strong southward directed winds suppress or even reverse this tidal residual flow. This effect is noticeable during stormy conditions with wind speeds exceeding 10 m/s. Onshore winds give near-bed offshore residual velocities (downwelling), counteracting the generally persistent density-driven effect. Offshore winds lead to near-bed onshore currents (upwelling), enhancing the density-driven effect.

Current and wind velocity measurements near Meetpost Noordwijk support these findings. Observations at this station indicate that southwestern storm winds of

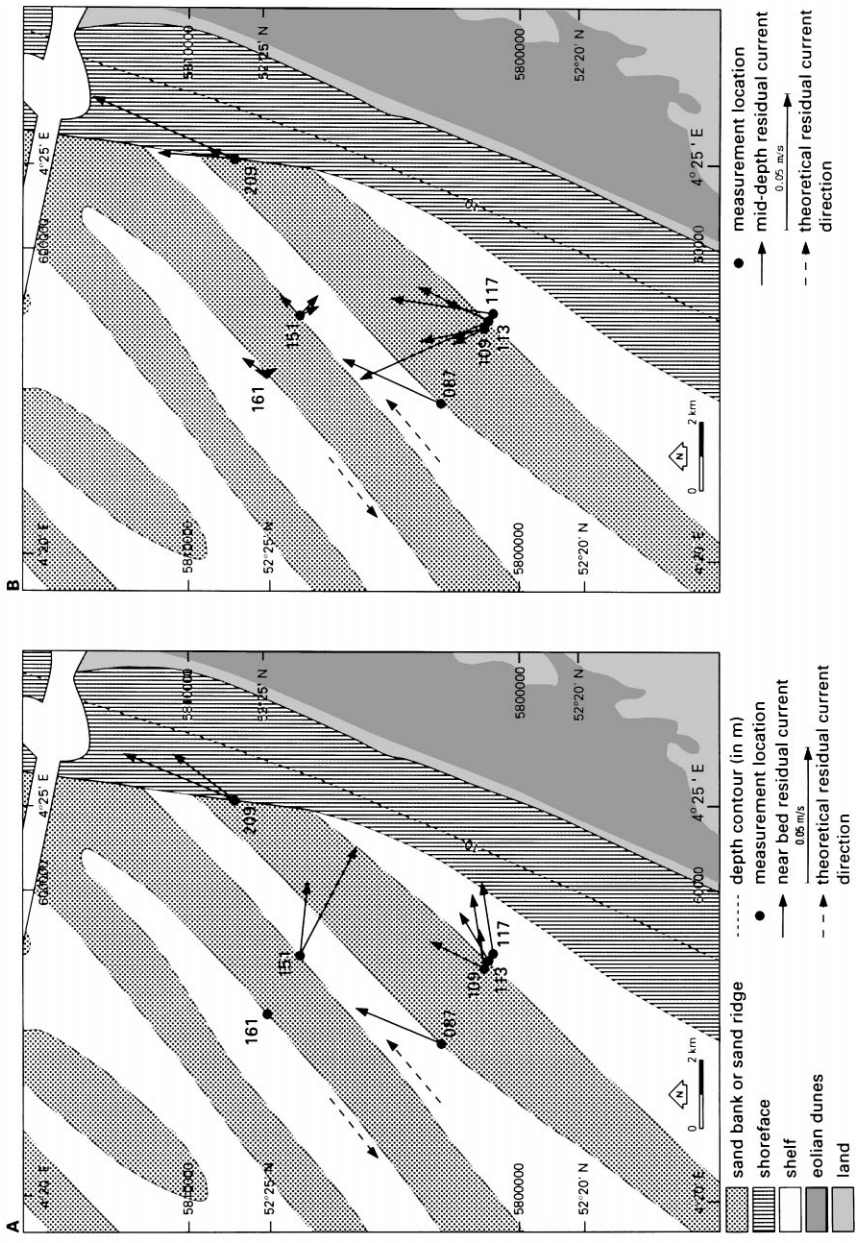

Fig. 5. Residual current velocities near the shoreface-connected ridges: (a) near-bed; and (b) mid-depth.

10 m/s result in 10% increase of longshore currents during the north-going flood and 10% decrease during the south-going ebb. Southwesterly winds of 15 m/s give 20% increase during flood and 20% decrease during ebb. Only storm winds from the south-west (wind sector 180–210°N) had a noticeable effect on the longshore componenent of the tidal current, winds from other directions had less impact.

The conclusion from these observations is that wind effects are noticeable only during incidental stormy conditions with wind speeds above 10 m/s. On average, winds between 10 and 15 m/s occur during 10 days per year (3% of the time) and winds of more than 15 m/s during 3 days per year (1% of the time). During the measurements, which focused on winter periods, these percentages amounted to 15 and 3%, respectively. Although wind affects the residual current pattern in the ways described above, the effects are considered incidental. Winds therefore may account partly for the variability observed in Fig. 5, but they are not expected to play a dominant role in this residual current pattern.

The residual current pattern was further analysed by separating local (morphology related) and regional effects (wind, density-gradients, Coriolis). This was done with the calculation of sum- and difference-records (cf. Howarth and Huthnance, 1984) from simultaneous observations at the two sides of the sand bank. The sum-record is defined here as $0.5(V_{\text{seaward}} + V_{\text{landward}})$, the difference-record as $0.5(V_{\text{seaward}} - V_{\text{landward}})$, where V is the residual cross- or along-bank velocity component at the seaward and landward side of the sand bank. When regional processes dominate the water motion, the mean values (sum-records) are expected to be maximal (equal to the average of the observations on each side of the bank), while the difference-records are expected to be minimal (the regional forcing is independent of the local topography). If local (morphology related) processes dominate the water motion, and the velocity parameters on each side of the sand bank are opposing and balancing, the reverse is expected: minimal sum-records and maximal difference-records. For all measurements discussed here, the sum-records are larger than the difference-records, which suggests that the residual current pattern around the ridges is dominated by regional processes and not by local (topographical) effects.

4.3. Wave observations

4.3.1. Experimental set-up

Wave velocity measurements during storm conditions were obtained during an experiment in December 1991, at deployment site MP 161 (Fig. 1). During the measurement period a couple of storms passed by with wind speeds up to 20 m/s (Beaufort 8–9), significant wave heights up to 4 m, peak wave periods between 8 and 9 s and near-bed wave orbital velocities up to 1.2 m/s. Since the winds during the peaks of the storms came predominantly from the west–northwest, the resulting wave field crossed the ridges approximately perpendicularly (Fig. 1). The measurements were done with a stand-alone instrumented tripod, equipped with electro-magnetic flow meters, optical backscatter sensors (OBSs) and a pressure sensor (Van de Meene, 1994). Typical results of the detailed (intra-burst) water and sediment motion at about 10 cm above the bed are given in Figs. 6(a), (b) and 7(a), (b). The detailed

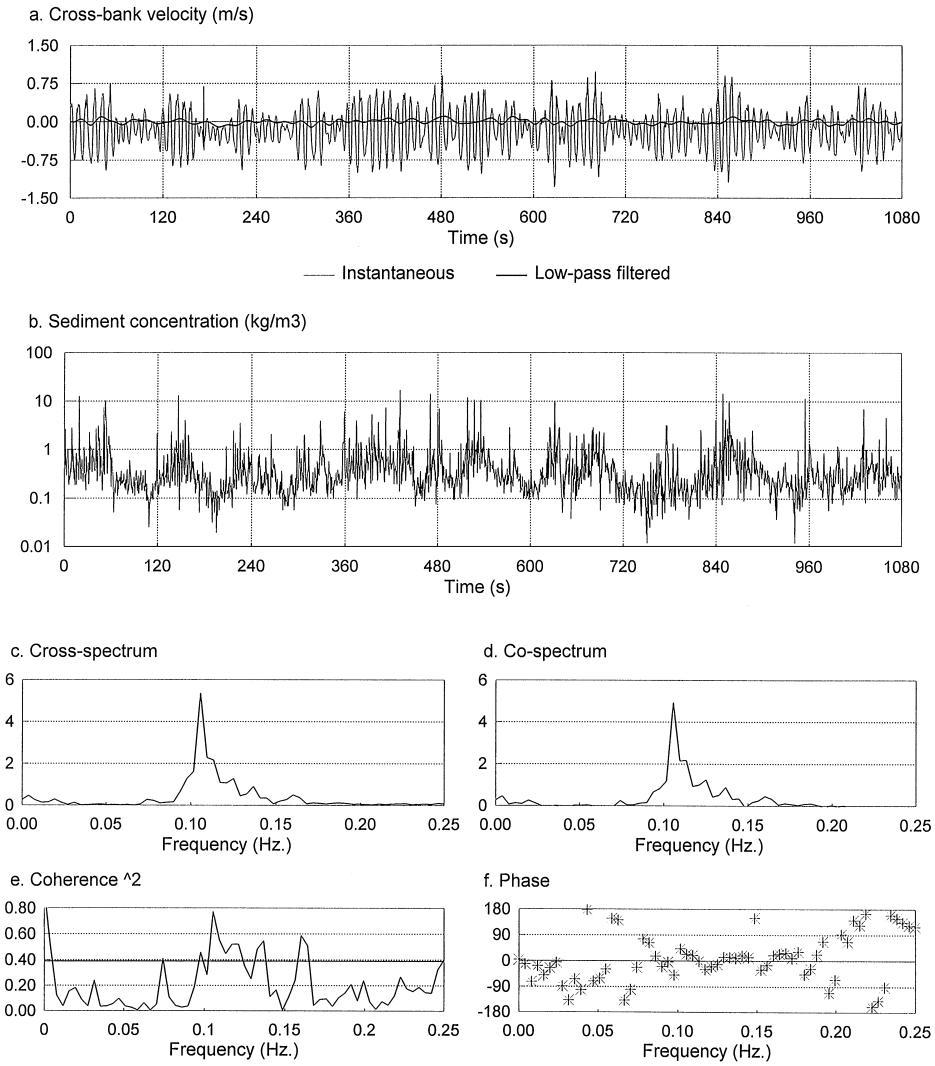

Fig. 6. Water and sediment motion during Burst 526 (18 December 1991, 13.00 CET; $H_s = 3.2$ m; $T_p = 7.7$ s). (a) instantaneous and low-pass filtered wave orbital velocity (u in m/s); (b) suspended sediment concentration (c in kg/m^3); (c) cross-spectrum uc ($S(f)$ in (kg/s m^2)^2/Hz); (d) co-spectrum of u and c ($S(f)$ in (kg/s m^2)^2/Hz); (e) squared coherence of cross-spectrum uc (-); and (f) phase difference between u and c (degrees).

sediment motion and the spectral analyses of these time-series will be discussed in Section 5.3.

4.3.2. Wave orbital velocities

The measured near-bed significant peak orbital velocities ($V_{s,crest}$ and $V_{s,trough}$) were compared with the theoretical values according to linear wave theory and

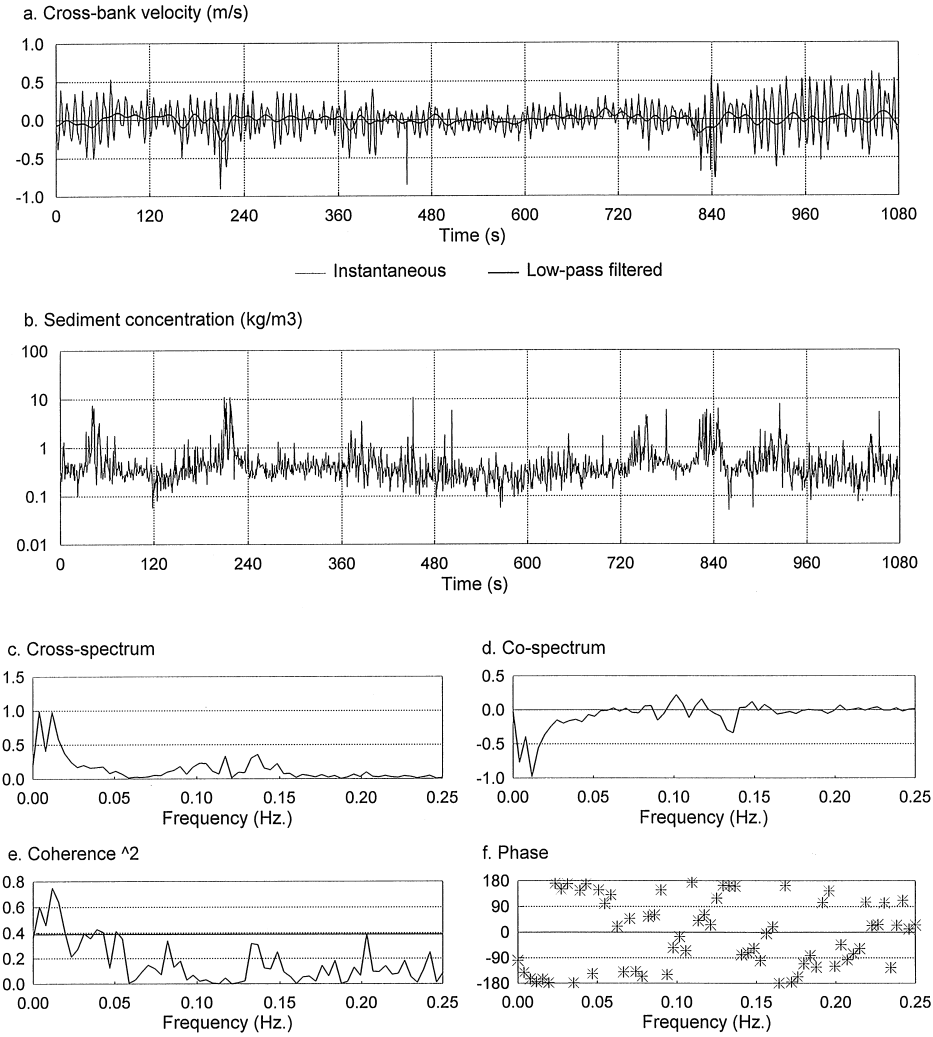

Fig. 7. Water and sediment motion during Burst 533 (18 December 1991, 20.00 CET; $H_s = 2.8$ m; $T_p = 7.6$ s): (a) instantaneous and low-pass filtered wave orbital velocity (u in m/s); (b) suspended sediment concentration (c in kg/m^3); (c) cross-spectrum uc ($S(f)$ in (kg/sm^2)^2/Hz); (d) co-spectrum of u and c ($S(f)$ in (kg/s m^2)^2/Hz); (e) squared coherence of cross-spectrum uc (-); and (f) Phase difference between u and c (degrees).

second-order Stokes, using $H_s (= H_{1/3})$ and T_p as input parameters. The significant peak velocity is defined here as the average of the highest third part of the observed instantaneous peak velocities during each burst. The actual water depths (14–18 m), wave heights (3–4 m) and wave periods (8–9 s) fell in the range where second- or third-order Stokes is expected to be valid.

Applying second-order Stokes indeed gives a reasonable agreement between the observed and the computed peak orbital velocities, although the calculated values

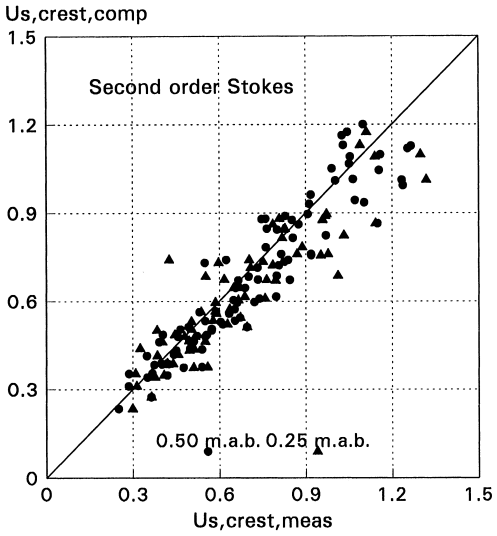

Fig. 8. Comparison between measured wave orbital velocities and wave orbital velocities calculated with second-order Stokes.

slightly underestimate the observations (Fig. 8). This underestimation increases with increasing orbital velocities, due to more intense shoaling of the waves. A higher-order Stokes, or an alternative approach, may give better fits at higher orbital velocities.

4.3.3. Wave asymmetry

The asymmetry ratio for the near-bed peak orbital velocity can be defined by

$$A_V = \frac{V_{\mathrm{s,crest}}}{V_{\mathrm{s,crest}} + V_{\mathrm{s,trough}}}, \tag{1}$$

where A_V is the asymmetry ratio (-), $V_{\mathrm{s,crest}}$ the significant current velocity under the wave crest (onshore, m/s), and $V_{\mathrm{s,trough}}$ the significant current velocity under the wave troughs (offshore, m/s).

The measured asymmetry ratio A_V is between 0.50 and 0.55 and independent of the wave orbital velocity V_s. This indicates that the wind waves were only slightly asymmetrical during the observed storm conditions. These results correspond with similar observations obtained on the Dutch shoreface near Egmond aan Zee.

4.3.4. Groupiness of the incident waves

Long waves in the offshore region may be either bound to the incident short waves or free travelling long waves. Offshore bound long waves result from non-linear interactions between interfering incident short waves.

Most time-series revealed a clear grouping of the incident orbital wave motion, suggesting the presence of free or bound long waves. Examples of such groupiness are

given in Figs. 6(a) and 7(a). Fig. 6(a) (burst 526) shows a very distinct groupiness; most time-series look similar. Fig. 7(a) (burst 533) is a special case. Waves are still grouped, but not as clear as in the previous example. Moreover, the time-series is not stationary on the burst time scale, with relatively low velocities between 400 and 820 s.

The *amount* of long-wave (infragravity) energy relative to the incident wave energy was determined from a spectral analysis of the velocity signal, while the *nature* of the observed groupiness was studied by analysing the phase relationship between the low-pass filtered velocity signal and the short-wave envelop (e.g. Roelvink, 1993). These analyses were done for the cross-bank velocity component, as this component corresponds roughly to cross-shore current velocities (see Fig. 1). Also, the incident waves crossed the banks more or less perpendicularly during the measurements.

The spectral analysis of the velocity signal revealed that the ratio between infragravity and incident wave energy varied between 0 and 5%. The amount of infragravity energy was thus relatively small, but in many cases not negligible. The infragravity peaks generally occurred at periods between 50 and 128 s. Burst 533 (Fig. 7(a)) formed an exception; in this burst the infragravity peak amounted to 12% of the incident wave peak energy, while it occurred at a period of 256 s.

The phase-relationship analysis revealed that bound long waves were present in about 50% of the time-series. Strikingly however, no bound long waves were observed in burst 526, despite the obvious grouping of the incident wave motion (Fig. 6(a)). In contrast, burst 533 revealed infragravity energy with a clearly bounded character, while grouping of the incident waves was less distinct (Fig. 7(a)).

Where bound long waves were present, the percentage of explained variance was up to 30%. This indicates that bound long waves were never dominant in the infragravity band. This finding corresponds to the conclusions drawn by Okhiro et al. (1992), who found that bound long waves contributed to less than 50% of the observed infragravity energy in water depths of 8–13 m and in a much smaller fraction in 183 m water depth. The remainder was explained by free (either leaky or edge) wave energy.

5. Sediment transport

5.1. Fair-weather sediment transport

5.1.1. Introduction

Fair-weather transport measurements were carried out at the crest of one of the shoreface-connected ridges, between locations 151 and 161 (Fig. 1), on 14 and 15 August 1990. The measurements were done with a Total Load Sampler, developed by Delft Hydraulics (Van Rijn and Gaweesh, 1992). The sampler was equipped with a bag-type bed load trap, a vertical array of intake nozzles connected to a series of pumps to obtain suspended sediment samples and three current meters (two propellers and one electromagnetic flow meter). The sampler allowed for the measurement of time-averaged sediment transport rates, based on direct sampling of the sediment.

The water depth at the measurement location varied between 13 and 15 m. Maximum depth-averaged currents were up to 0.8 m/s. During the measurements,

the weather was fair, with a significant wave height between 0.3 and 0.8 m and a wave period of 4 s.

5.1.2. Observations

The small-scale morphology superimposed on the large ridges was determined from side scan sonar surveys, echosoundings and video observations. The small-scale bed forms consisted of megaripples with an average length of 10 m and an average height of 0.2–0.3 m, covered with small-scale ripples with a length of 0.2 m and a height in the order of a few cm (echosounding observations). The crests of the megaripples were generally oriented more or less perpendicular to the dominant flood tidal current. The bedforms did not show any indication for veering of the currents towards the bank crests.

A selection of the current velocity and bed load and suspended load transport rates is given in Fig. 9 (15 August 1990, morning). The observed sediment transport rates were small and occurred only during a period of about 2 h around maximum flow of the flood phase. Near-bed current velocities (0.45 m above the bed) were around 0.4 m/s. The observed suspended sediment concentrations were very low, with a maximum value of 40 mg/l at 0.07 m above the bed.

The suspended load transport rates, extrapolated over the vertical, are given in Fig. 9 as well. The suspended load transport rates are slightly smaller than the bed load transport rates. The period during which sediment is transported in suspension is also shorter than the bed load transport period (1 h). This leads to the conclusion that

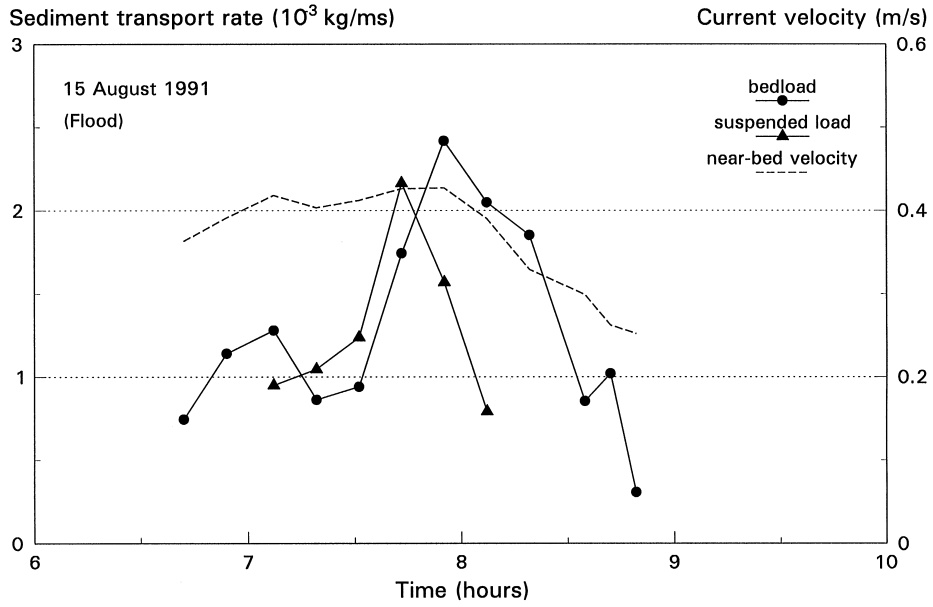

Fig. 9. Near-bed current velocity, bed load and suspended load transport during spring tide flood (15 August 1990).

bed load is dominant at low tidal velocities, whereas the total fair-weather transport is highly episodic. There is a small, but striking phase difference between the two types of sediment transport, with the bed load lagging behind the suspended load transport. This phase difference may be related to the actual position of the measurement frame relative to the megaripple morphology (trough, crest, lee- or stoss-side). Since we could not assess the exact position of the frame relative to the ripple morphology during the experiment and since we could only take a limited amount of measurements, we cannot draw any conclusion regarding this phase difference.

5.1.3. Comparison with other field experiments

Most measurements of sediment transport rates on the continental shelf have been based on tracer experiments and on bed form migration rates in modern and ancient environments. Van Veen (1936) discusses bed load measurements in the Straits of Dover and around the Varne sand bank. These measurements actually are suspended sediment *fluxes* (in kg/m^2 s) at 0.1 m above the bed. Hardisty and Hamilton (1984) describe bed load transport *rates* (in kg/m s), obtained with sediment traps deployed on the continental shelf off Lands End (UK) in a water depth of approximately 100 m. The sea bed was covered with low-amplitude bed forms (sand ribbons and sand patches) and the mean grainsize varied between 54 and 287 μm.

The results of the different experiments are summarized in Table 2. The sediment *fluxes* observed by Van Veen (1936) and Van de Meene and Van Rijn (1994) are small and in the same order of magnitude. The sediment transport *rates* observed by Hardisty and Hamilton (1984) are a factor 20 smaller than the Zandvoort observations, which may be explained by the differences in water depth and subsequent differences in wave action and current strength.

All observations are under conditions close to the beginning of sediment motion. Under these conditions, the sediment transport rate is very sensitive to the current velocity, which may explain the observed differences.

Table 2
Summary of fair-weather sediment transport measurements in the North Sea[a]

Reference	Location	h (m)	d_{50} (mm)	u_b (m/s)	h_{meas} (m)	Rate (kg/m s)	Flux (kg/m^2 s)
Van Veen (1936)	Dover Strait	30	—	—	0.1	—	0.001
	Varne Bank	30	—	—	0.1	—	0.008
Hardisty and Hamilton (1984)	Lands End	100	0.05–0.30	0.24–0.30	—	0.0001	—
Van de Meene and Van Rijn (1994)	Zandvoort	14	0.25–0.30	0.4	0.07	0.002	0.004–0.02

[a] h = water depth; d_{50} = median grainsize; u_b = near-bed current velocity; h_{meas} = measurement height above the bed; rate = sediment transport rate; and flux = sediment flux.

5.1.4. Residual sand transport

As a result of the asymmetry of the tidal current velocity and the non-linear transport-velocity relationship, the residual current pattern will generally not coincide with the residual sediment transport pattern. This is illustrated in Fig. 10, where the near-bed residual velocity (1 m.a.b.) of one of the time-series discussed in Section 4.2 (MP 151, January–February 1991, Fig. 5) is compared with the residual sediment transport direction calculated from the same time-series. The residual sediment transport vector was calculated with a function of the form

$$S = a(V - V_{\text{crit}})^b, \tag{2}$$

where S is the sediment transport vector, a an arbitrary constant, V the measured current velocity, V_{crit} the critical current velocity below which sediment transport is zero, and b a power.

For the present discussion, the absolute magnitude of the sediment transport is irrelevant, so a was set to 1. The power b was taken 3, which is a common value for sediment transport formulae. The threshold velocity V_{crit} follows from the measurements and was set at 0.45 m/s.

The residual current velocity presented in Fig. 10 amounts to 0.03 m/s and is directed 96°N, i.e. towards the coast. This was a persistent shoreward directed residual for a period of two months, reflecting a persistent estuarine type of circulation (Section 4.2). The associated residual sediment transport is directed 15°N, i.e. parallel to the coast, northwards with the dominant flood tidal current. The effect of V_{crit} is relatively small: with V_{crit} set at 0 m/s, the residual transport direction is 30°N. This

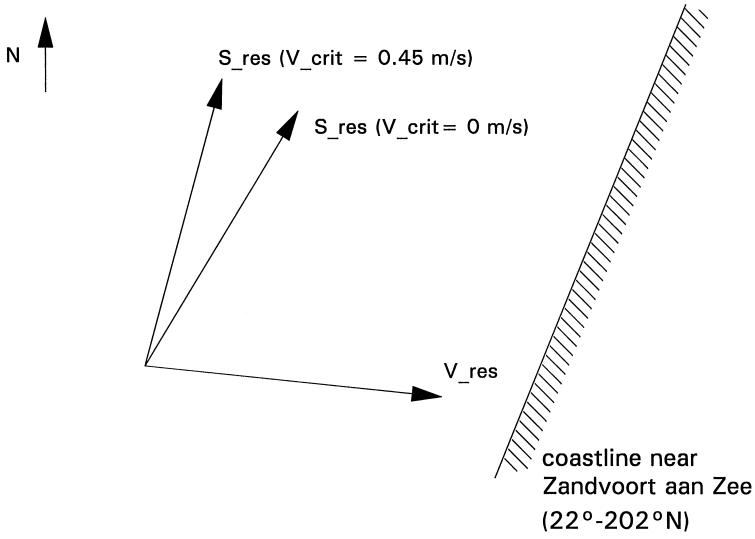

Fig. 10. Comparison of the residual velocity vector with the calculated residual sediment transport vector ($S \sim (V - V_{\text{crit}})^3$).

indicates that also when wave stirring reduces the threshold velocity, the residual sediment transport direction will still be aligned predominantly with the flood tidal current. Comparable results were obtained by Gao and Collins (1997).

5.2. Sediment transport during storms

5.2.1. Introduction

Sediment transport measurements have also been collected during the experiment in December 1991 at site MP 161 (Fig. 1, Section 4.3). Suspended sediment concentrations were obtained with optical backscatter sensors (OBS). A particular problem during the experiment was the determination of the height of the OBSs above the bed. This height may vary due to settling of the frame and migration of bedforms. It was assumed that the lower OBS was located approximately at the sea bed when the amount of overflow data in a burst ranged between 20 and 2140 values (between 1 and 99%). Under these conditions, the lower sensor was alternatingly exposed (above the sea bed) and buried. Consequently, the upper OBS during these specific bursts was at a relatively well-defined and constant level of about 0.1 m above the sea. Of a total of 74 bursts, 20 met these conditions. These data were used for the analyses presented below.

5.2.2. Mean-, high- and low-frequency sediment fluxes

The instantaneous measurements of velocity and suspended sediment concentration were decomposed into a mean and an oscillating component; the oscillating part, in addition, was split into short- and long-periodic components. As a result, the total time-averaged cross- and along-bank sediment fluxes $\langle cu \rangle$ and $\langle cv \rangle$ were split into a mean flux component and several oscillating flux components:

$$\langle u \cdot c \rangle = \bar{u} \cdot \bar{c} + \langle \tilde{u}_s \cdot \tilde{c}_s \rangle + \langle \tilde{u}_L \cdot \tilde{c}_L \rangle + \langle \tilde{u}_s \cdot \tilde{c}_L \rangle + \langle \tilde{u}_L \cdot \tilde{c}_s \rangle (\mathrm{kg/m^2\ s}), \tag{3}$$

$$\langle v \cdot c \rangle = \bar{v} \cdot \bar{c} + \langle \tilde{v}_s \cdot \tilde{c}_s \rangle + \langle \tilde{v}_L \cdot \tilde{c}_L \rangle + \langle \tilde{v}_s \cdot \tilde{c}_L \rangle + \langle \tilde{v}_L \cdot \tilde{c}_s \rangle (\mathrm{kg/m^2\ s}), \tag{4}$$

where u, v are the cross- and along-bank wave orbital velocities (m/s), c is the sediment concentration (kg/m^3), $\bar{u}$, $\bar{v}$, $\bar{c}$ are the time-averaged values, $\tilde{u}_s$, $\tilde{v}_s$, $\tilde{c}_s$ are the high-frequency oscillations, and $\tilde{u}_L$, $\tilde{v}_L$, $\tilde{c}_L$ are the low-frequency oscillations.

For the present study, the brackets $\langle\ \rangle$ in Eqs. (3) and (4) indicate time-averaging over 18 min. The long- and short-periodic components were obtained by low- and high-pass filtering the instantaneous time-series with a cut-off frequency of 0.05 Hz, which is at a spectral trough in the studied time-series. This cut-off frequency is approximately twice the maximum observed peak incident wave period. A set of six fluxes were obtained: a total flux, consisting of a mean and four oscillatory fluxes. The mean flux direction, by definition, corresponds to the mean current direction. In the inner-shelf environment, this mean current is a combination of tide-, wind- and density-driven flows, with the Coriolis effect acting on all these currents. The short-wave flux represents the net effect of the sediment fluxes induced by the incident wave orbital motion. The long-wave oscillatory flux is associated with bound long waves.

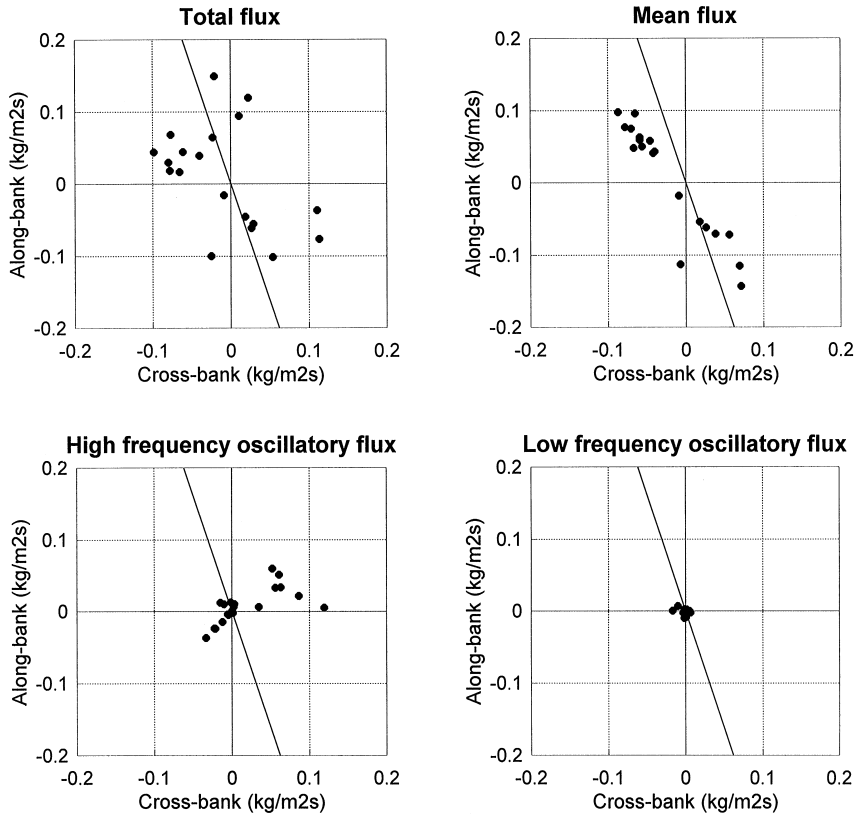

Fig. 11. Sediment fluxes. Solid line in the figure indicates coastline; bank-axis corresponds with Y-axis.

The short wave–long wave interaction terms were found to be zero, indicating that $\tilde{u}_s$ and $\tilde{u}_L$ are not correlated with $\tilde{c}_L$ and $\tilde{c}_s$ respectively.

The results of the 20 selected bursts are given in Fig. 11. In general, the mean fluxes $\overline{u}\overline{c}$ and $\overline{v}\overline{c}$ are dominant. The short-wave oscillatory fluxes are variable in magnitude and direction. Although generally somewhat smaller than the mean fluxes, they cannot be neglected. Superimposed on the mean fluxes, they give significant differences between the mean and the total sediment fluxes. The largest non-zero wave oscillatory fluxes occur under more energetic conditions ($V_s > 0.7$ m/s). The largest fluxes are positive, directed landwards (Fig. 11). The results indicate that wave stirring and advection by the mean current are the dominant sediment transporting processes. The long-wave oscillatory fluxes are an order of magnitude smaller and sometimes negligible. The long-wave-induced, seaward directed sediment transport on continental shelves may in part be present here, albeit very small. It has not been possible to establish the effect of bed topography on the observed oscillatory flux directions.

5.2.3. Details of the water and sediment motion

Figs. 6(b) and 7(b) present the detailed sediment characteristics of Bursts 526 and 533. The 'grassy' character (peakedness) of the suspended sediment time-series may be partly due to the measurement method. The OBSs may give very high readings when debris or shell fragments pass the sensor at short distance, giving erratic peaks. Bursts 526 and 533 both reveal an obvious correlation of bursts of suspension with groups of large waves (Figs. 6(a), (b) and 7(a), (b)). However, the characteristics of the two bursts differ, as is evident from the spectral analyses (Figs. 6(d)–(f) and 7(d)–(f)).

The cross-spectra (Figs. 6(c) and 7(c)) give the spectral density of the sediment flux uc, while the co-spectra (Figs. 6(d) and 7(d)) provide the correlation between u and c at different frequencies. The squared coherence (Figs. 6(e) and 7(e)) forms a measure for the statistical significance of the cross-spectral peaks. For the present analysis, cross-spectral peaks are significant when the squared coherence is larger than 0.39 ($\alpha = 0.05$). The phase angles (Figs. 6(f) and 7(f)) indicate whether u and c are in phase (0°) or out phase ($\pm 180^\circ$) at different frequencies.

In Burst 526 (Fig. 6), storm waves dominate the entire spectrum. Despite the distinct grouping of the velocity and sediment signal, the amount of infragravity energy is less than 1% of the incident wave energy. Incoming waves stir-up the sediment, as is evident from the cross- and co-spectral peaks and the zero-phase difference at the incident wave frequency (Figs. 6(c), (d) and (f)). Despite the obvious correlation of bursts of suspension with groups of large waves, the analysis of the velocity signal (Section 4.3) has shown that bound long waves are negligible. This is confirmed by the co-spectrum, which shows little correlation between u and c at the infragravity wave scale (Fig. 6(d)).

Burst 533 (Fig. 7) reveals velocity and concentration variations at periods in the order of 300 s. These fluctuations are reflected in the cross-spectrum as well (Fig. 7(c)). The co-spectrum indicates that u and c are negatively correlated and out of phase ($\pm 180^\circ$) at the long-wave scale (Figs. 7(d) and (f)). These oscillations therefore have the characteristics of bound long waves, confirming the outcome of the analysis of the velocity signal (Section 4.3). However, their period is rather long (spectral peak at 256 s). If the bound long waves were tied to the incident waves, a long-wave period of about 60–70 s (i.e. approximately seven times the incident wave period) would be more obvious. An explanation for the observed sediment fluxes at a time scale of minutes is not available. Additional information on the bed morphology, which might provide an answer, is lacking. The velocity time-series obtained at 0.25 m above the one shown in Fig. 7(a) reveals the same fluctuations, indicating that the observations are more than an anomaly restricted to one sensor.

Other bursts with bound long waves in the velocity signal revealed small, but negative and out-of-phase correlations at infragravity wave periods between 50 and 128 s. No significant coherence was observed at twice the incident wave frequency. This indicates that the correlation between u and c (i.e. the wave fluxes) are not in quadrature, but random (Hanes and Huntley, 1986).

6. Discussion and conclusions

6.1. Hydrodynamics

The long-term residual current pattern in the study area appears to be controlled by the northwards directed dominant flood current and by persistent density-driven effects. These results are consistent with other studies in the area (Van der Giessen et al., 1990; Van de Meene, 1994). Possibly, these regional effects dominate potential weak morphologically induced residual currents.

The ADCP observations have revealed an along-bank velocity decrease and a cross-bank velocity increase, which is expected from theory. However, the observed response agrees only partially and only qualitatively with theory. The response is relatively clear during ebb and less clear during flood.

The residual current pattern observed at various locations in the ridge area does not reveal any evidence for morphological steering induced by the ridges. Although the tidal current veers towards the ridge crest, the expected consistent decrease in current velocity across the ridges, and the associated residual circulation around the ridges, are absent. There are no indications for vertical residual circulations either.

Horizontal residual circulations around tidal sand banks have been observed by many authors (e.g. Heathershaw and Hammond, 1980; Howarth and Huthnance, 1984; Pattiaratchi and Collins, 1987; Collins et al., 1995). In all cases, the circulation was clockwise around the ridges. The observed horizontal circulations are generally only indicative, due to lack of sufficient field data. Other studies did not observe such residual circulations (e.g. Harris et al., 1992; Klein and Mittelstaedt, 1992; Antia et al., 1995). Vertical residual circulations were observed occasionally (Heathershaw and Hammond, 1980; Pattiaratchi and Collins, 1987). The oblique orientation of the sand banks with respect to the dominant current and the veering of the current toward the crest are observed in most of the above field studies on linear sand banks, including the present one.

Based on current measurements, Klein and Mittelstaedt (1992) argued that storm-driven flows could be the only mechanism responsible for the formation of the shoreface-connected ridges on the East-Frisian shelf off the German coast, since fair-weather sediment transport rates are supposed to be very low. This conclusion is rather premature, since their data do not give any indication if and how storm-driven flows may contribute to the formation of these ridges. In contrast, Antia et al. (1995) concluded for the same area that sediment transport may be significant during fair-weather conditions. However, although they observed some spatial velocity variations, which they related to the ridge morphology, they found no consistent velocity patterns supporting the aforementioned theories of ridge formation and maintenance.

Swift and Field (1981) present a brief review of measurements near shoreface-connected ridges on the Atlantic shelf off the east coast of the USA. Hydrodynamic field observations were restricted to several incidental current meter deployments near some of the ridges. Due to the weak tidal currents, the sediment transport is very episodic, being related to the occurrence of northeastern (winter-) storms. The

net sediment transport was directed towards the south. Although storm-driven flows seem to be important on the American shelf, their role in the formation and the maintenance of the shoreface-connected ridges remains obscure. The present data do not give any evidence that such storm-driven flows play a dominant role.

The observations on the short- and long-wave fields around the ridges (Sections 4.3 and 5.2) give no positive indication that models based on the non-linear response of the wave field, as proposed by Boczar-Karakiewicz and Bona (1986) and Boczar-Karakiewicz et al. (1990, 1991), might apply to the shoreface-connected ridges along the Dutch coast.

The field studies mentioned above provide at most partial support for the theoretical flow pattern that is expected from the bed-instability models. In particular, none of the studies discuss the expected deceleration of the along-bank velocity component and the associated sedimentation at the ridge crest (Part 2 of this paper; Van de Meene and Van Rijn, 2000). It is therefore concluded, on the basis of the present study as well as on the studies mentioned above, that the applicability of the bed-instability models (Huthnance, 1982; De Vriend, 1990; Hulscher, 1993) is not (yet) sufficiently supported by field observations.

On the other hand, the field data do not falsify the basic approach which all morphodynamic models have in common, viz. to consider sand bank systems as manifestations on the inherent instability of the morphodynamic system. In fact, sedimentological observations near the shoreface-connected ridges support this basic approach, as they have demonstrated that the ridges were formed in a morphodynamic setting comparable to the present one, while they have also shown that the ridges are still active (Van de Meene, 1994).

Possible explanations for the discrepancies between observations and theory are the finite length of the ridges, the gentle slopes of the ridges, the presence of the coastline, the fact that the ridges are connected to the shoreface and the gentle, but regional slope of the sea bed.

6.2. Sediment transport

Sediment transport observations during spring tidal, fair-weather conditions have shown that the sediment transport rates under these conditions are very low and occur only during a period of about 2 h around maximum tidal flow. Bed load transport is slightly dominant. As a result of the episodic character of the fair-weather sediment transport, there is a significant deviation between the net current direction and the net sediment transport direction.

The sediment transport measurements during storm conditions have revealed a large variability in transport directions. Although the mean fluxes dominate the sediment mobility during storms, the contribution of short-wave oscillatory fluxes to the total flux cannot be neglected. Long-wave oscillatory fluxes are negligible.

There are very few studies giving detailed information on sediment suspension processes on a sandy inner-shelf. Wright et al. (1991) have done an extensive study on sediment transport processes in the sandy shoreface environment along the east coast of USA, in water depths generally around 10 m and with a maximum of 17 m.

Comparable to the data presented in this paper, Wright et al. (1991) find the mean sediment fluxes to be the most important contributor to the total sediment flux. This was the case for a variety of different conditions, ranging from fair-weather to storms. Incident waves were important for stirring up the sediment. As in the present study, oscillatory fluxes were directed onshore as well as offshore. According to Wright et al. (1991), this variety in direction may be explained by phase lags between $u(t)$ and $c(t)$, caused by the presence of small-scale ripples. Low-frequency effects were measurable, but not dominant. Low-frequency fluxes were directed landward as well as seaward.

Green et al. (1995) describe the results of an experiment in the British part of the North Sea, in water depths of 25 m. Their OBS data revealed advection of sediment clouds past the sensor, wave resuspension of bed sediments and modulation of sediment concentration by wave groups. At 0.34 m above the bed (compared to 0.10 m for the Zandvoort measurements), wave oscillatory fluxes were small compared to the mean flux but not negligible. Mean suspended sediment concentrations during a severe storm were in the order 0.3–0.5 kg/m^3, an order of magnitude smaller than ours. The Zandvoort data generally showed stronger wave oscillatory fluxes, which may be explained by the fact that our measurements were taken in shallower water and closer to the sea bed.

Acknowledgements

This study was done within the framework of the Coastal Genesis Programme and was partly funded by the National Institute for Coastal and Marine Management (RIKZ) of the Ministry of Transport, Public Works and Water Management. Technical assistance for the measurements was provided by the Department of Physical Geography, Utrecht University. The crew of the RV *Professor Lorentz* skillfully handled the instruments at sea. We appreciate the useful comments of the reviewers on earlier versions of this paper.

References

Antia, E.E., Flemming, B.W., Wefer, G., 1995. Calm-weather spring and neap tidal current characteristics on a shoreface-connected ridge complex in the German Bight (southern North Sea). Geo-Marine Letters 15, 30–36.

Belderson, R.H., 1986. Offshore tidal and non-tidal sand ridges and sheets: differences in morphology and hydrodynamic setting. In: Knight R.J., McLean, J.R. (Eds.), Shelf Sands and Sandstones, Canadian Society of Petroleum Geologists, Memoir II, pp. 293–301.

Boczar-Karakiewicz, B., Amos, C.L., Drapeau, G., 1990. The origin and stability of sand ridges on Sable Island Bank, Scotian Shelf. Continental Shelf Research 10, 683–704.

Boczar-Karakiewicz, B., Bona, J.L., 1986. Wave-dominated shelves: a model for sand ridge formation by progressive infragravity waves. In: Knight, R.J., McLean, J.R. (Eds.), Shelf Sands and Sandstones. Canadian Society of Petroleum Geologists, Memoir II, pp. 163–179.

Boczar-Karakiewicz, B., Bona, J.L., Pelchat, B., 1991. Interaction of internal waves with the sea bed on continental shelves. Continental Shelf Research 11, 1181–1197.

Collins, M.B., Shimwell, S.J., Gao, S., Powell, H., Hewitson, C., Taylor, J.A., 1995. Water and sediment movement in the vicinity of linear sand banks: the Norfolk Banks, Southern North Sea. Marine Geology 123, 125–142.

De Vriend, H.J., 1990. Morphological processes in shallow tidal seas. In: Cheng, R.T. (Ed.), Coastal and Estuarine Studies, Vol. 38, Residual Currents and Long-term Transport, Springer, Berlin, pp. 276–301.

De Vriend, H.J., Zyserman, J., Nicholson, J., Roelvink, J.A., Péchon, P., Southgate, H.N., 1993. Medium-term 2DH coastal area modelling. Coastal Engineering 21, 193–224.

Dyer, K.R., Huntley, D.A., 1999. The origin, classification and modelling of sand banks and sand ridges. Continental Shelf Research 19, 1285–1330.

Gao, S., Collins, M.B., 1997. Changes in sediment transport rates caused by wave action and tidal flow time-asymmetry. Journal of Coastal Research 13, 198–201.

Godin, G., 1972. The Analysis of Tides. Liverpool University Press, Liverpool, 264pp.

Green, M.O., Vincent, C.E., McCave, I.N., Dickson, R.R., Rees, J.M., Pearson, N.D., 1995. Storm sediment transport: observations from the British North Sea shelf. Continental Shelf Research 15, 889–912.

Hanes, D.M., Huntley, D.A., 1986. Continuous measurements of suspended sand concentration in a wave-dominated nearshore environment. Continental Shelf Research 6, 585–596.

Hardisty, J., Hamilton, D., 1984. Measurements of sediment transport on the sea bed southwest of England. Geo-Marine Letters 4, 19–23.

Harris, P.T., Pattiaratchi, C.B., Cole, A.R., Keene, J.B., 1992. Evolution of subtidal sandbanks in Moreton Bay, Eastern Australia. Marine Geology 103, 225–247.

Heathershaw, A.D., Hammond, F.D.C., 1980. Secondary circulations near sand banks and in coastal embayments. Deutsche Hydrographische Zeitschrift 33, 135–151.

Houbolt, J.J.H.C., 1968. Recent Sediments in the Southern Bight of the North Sea. Geologie en Mijnbouw 47, 245–273.

Howarth, M.J., Huthnance, J.M., 1984. Tidal and Residual Currents around a Norfolk Sandbank. Estuarine, Coastal and Shelf Science 19, 105–117.

Hulscher, S.J.M.H., 1996. Formation and migration of large-scale, rhythmic sea-bed patterns: a stability approach. Ph.D. Thesis, Institute of Marine and Atmospheric Research, Utrecht University, 143pp.

Hulscher, S.J.M.H., De Swart, H.E., De Vriend, H.J., 1993. The generation of offshore tidal sand banks and sand waves. Continental Shelf Research 13, 1183–1204.

Huthnance, J.M., 1982. On one mechanism forming linear sand banks. Estuarine, Coastal and Shelf Science 14, 79–99.

Klein, H., Mittelstaedt, E., 1992. Local currents at a shoreface-connected ridge in the German Bight. Deutsche Hydrographische Zeitschrift 44, 133–142.

Laban, C., Schüttenhelm R.T.E., 1981. Some new evidence on the origin of the Zeeland ridges. In: Nio, S.D., Schüttenhelm, R.T.E., van Weering, Tj.C.E. (Eds.), Holocene Marine Sedimentation in the North Sea Basin. Special Publication of the International Association of Sedimentologists, Vol. 5, pp. 239–246.

McBride, R.A., Moslow, T.F., 1991. Origin, evolution, and distribution of shoreface sand ridges, Atlantic inner shelf, USA. Marine Geology 97, 57–85.

McCave, I.N., 1979. Tidal currents at the North Hinder Lightship, Southern North Sea: flow direction and turbulence in relation to maintenance of sand banks. Marine Geology 31, 101–114.

Off, T., 1963. Rhythmic linear sand bodies caused by tidal currents. Bulletin of the American Association of Petroleum Geologists 47, 324–341.

Okhiro, M., Guza, R.T., Seymour, R.J., 1992. Bound infragravity waves. Journal of Geophysical Research 97, 11453–11469.

Pattiaratchi, C.B., Collins, M., 1987. Mechanisms for linear sandbank formation and maintenance in relation to dynamical oceanographic observations. Progress in Oceanography 19, 117–176.

Roelvink, J.A., 1993. Surf beat and its effect on cross-shore profiles. Ph.D. Thesis, Technical University Delft, 116pp.

Stubblefield, W.L., McGrail W., Kersey, D.G., 1984. Recognition of transgressive and post-transgressive sand ridges on the New Jersey Continental shelf. SEPM Special Publication 34, Soc. Econ. Paleont. Mineral Tulon, pp. 1–23.

Swift, D.J.P., Field, M.E., 1981. Evolution of a classic sand ridge field: Maryland sector, North America inner shelf. Sedimentology 28, 461–482.

Swift, D.J.P., Parker, G., Lanfredi, N.W., Perillo, G., Figge, K., 1978. Shoreface-connected sand ridges on American and European shelves: a comparison. Estuarine and Coastal Marine Science 7, 257–273.

Van de Meene, J.W.H., 1994. The shoreface connected ridges along the central Dutch coast. Ph.D. Thesis, KNAG/Netherlands Geographical Studies 174, Utrecht, the Netherlands, 222pp.

Van de Meene, J.W.H., Van Rijn, L.C., 1994. Tide- and stormdriven sediment transport on the inner-shelf along the Dutch coast. Proceedings Coastal Dynamics'94. ASCE, New York, pp. 822–836.

Van de Meene, J.W.H., Van Rijn, L.C., 2000. The shoreface-connected ridges along the central Dutch coast — part 2: morphological modelling. Continental Shelf Research 20, 2325–2345.

Van der Giessen, A., de Ruijter, W.P.M., Borst, J.C., 1990. Three-dimensional current structure in the Dutch coastal zone. Netherlands Journal of Sea Research 25, 45–55.

Van Rijn, L.C., 1997. Sediment transport and budget of the central coastal zone of Holland. Coastal Engineering 32, 61–90.

Van Rijn, L.C., 1998. Principles of Coastal Morphology. Aqua Publications, Amsterdam, The Netherlands.

Van Rijn, L.C., Gaweesh, M.T.K., 1992. New total sediment-load sampler. Journal of Hydraulic Engineering 118, 1686–1691.

Van Veen, J., 1936. Onderzoekingen in de hoofden in verband met de gesteldheid der Nederlandse kust. Algemeene Landsdrukkerij, Den Haag, 252pp.

Wright, L.D., 1995. Morphodynamics of Inner-Continental shelves. Marine Science Series, CRC Press, Boca Raton, FL, 233pp.

Wright, L.D., Boon, J.D., Kim, S.C., List, J.H., 1991. Modes of cross-shore sediment transport on the shoreface of the Middle Atlantic Bight. Marine Geology 96, 19–51.